RESEARCH ARTICLE

SusMat WILEY

In situ electrochemical synthesis of atomically dispersed metal sites for efficient hydrogen evolution reaction

Tingting Liu[1,2] | Zonghua Pu[1] | Zhangsen Chen[1] | Mingjie Wu[1] | Yongpeng Xia[1] | Sixiang Liu[1] | Ning Chen[3] | Weifeng Chen[3] | Lei Zhang[4] | Zhangxing Chen[5] | Gaixia Zhang[2] | Shuhui Sun[1]

[1]Institut National de la Recherche Scientifique (INRS), Center Énergie Matériaux Télécommunications, Varennes, Québec, Canada

[2]Department of Electrical Engineering, École de Technologie Supérieure (ÉTS), Montréal, Québec, Canada

[3]Canadian Light Source (CLS), Saskatoon, Saskatchewan, Canada

[4]Energy, Mining and Environment, National Research Council of Canada, Vancouver, British Columbia, Canada

[5]Department of Chemical and Petroleum Engineering, University of Calgary, Calgary, Alberta, Canada

Correspondence
Zhangxing Chen, Department of Chemical and Petroleum Engineering, University of Calgary, Calgary, Alberta, T2N 1N Canada.
Email: zhachen@ucalgary.ca

Gaixia Zhang, Department of Electrical Engineering, École de Technologie Supérieure (ÉTS), Montréal, Québec, H3C 1K3 Canada.
Email: gaixia.zhang@etsmtl.ca

Shuhui Sun, Institut National de la Recherche Scientifique (INRS)-Center Énergie Matériaux Télécommunications, Varennes, Québec, J3X 1P7 Canada.
Email: shuhui.sun@inrs.ca

Abstract

The development of efficient and robust non-Pt and low-Pt catalysts with equivalent or even superior performance to commercial Pt-based catalysts for hydrogen evolution reaction (HER) is highly desired, but challenging, in the field of water electrolysis. Herein, we report a facile and cost-effective in situ electrochemical approach for the synthesis of atomically dispersed metal sites including platinum (Pt), ruthenium (Ru), and palladium (Pd) on the polyaniline (PANI) support. The PANI exhibits not only high electrochemical conductivity but also efficient H^+ capture from hydronium ions, leading to the formation of protonated amine groups that can be easily electrochemically reduced to H_2 on atomically dispersed metal active sites. As an example, the atomically dispersed Pt sites anchored on carbon cloth-supported PANI (PANI-Pt/CC) demonstrate excellent activity and durability toward the HER. The mass activity of PANI-Pt-10/CC reaches 25 A mg_{Pt}^{-1}, exhibiting a significant enhancement of 50-fold compared to that of the commercial Pt/C (0.5 A mg_{Pt}^{-1}). Therefore, this study presents a universally applicable approach for the design of atomically dispersed metal sites/conducting polymer heterostructures for highly efficient catalysts toward HER and beyond.

KEYWORDS
electrocatalyst, hydrogen evolution, in situ reduction, PANI nanofiber, single-atom catalyst

1 | INTRODUCTION

Water splitting constitutes the principal process in clean energy technologies,[1–6] such as proton exchange membrane water electrolyzers, anion exchange membrane water electrolyzers and conventional alkaline water electrolyzers. Hydrogen evolution reaction (HER) plays a pivotal role in the process of water splitting for sustainable hydrogen generation. However, the utilization of rare and high-cost platinum-group-metal catalysts seriously limits the widespread commercialization of these clean energy devices.[7–12] In this context, significant efforts have been dedicated to the development of non-Pt and low-Pt electrocatalysts for HER.

On one hand, in recent years, there have been great advancements in the development of earth-abundant non-Pt materials (Fe-, Co-, Ni-, Mo-, Cu-, W-, Al-, Zn-, and Mn-based compounds) for efficient HER catalysis in acidic, neutral and alkaline solutions.[13–23] Nevertheless, for the non-noble compounds, it remains a big challenge to achieve a Pt-like catalytic activity. On the other hand, lowering the dosage of Pt, and using supported Pt nanoparticles (Pt NPs) on a substrate is a general way to increase the Pt catalytic activity and improve the utilization efficiency. However, the geometry of nanoparticles restricts the majority of the Pt atoms to reside in the particle core, rendering them ineffective for catalytic reactions as only the surface atoms participate in the chemical processes.[24] Theoretically, downsizing platinum particles to individual atoms represents one of the most effective strategies for improving Pt utilization efficiency and consequently reducing catalyst material costs.[25] The efficiency of single-atom catalysts (SACs), characterized by the dispersion of isolated individual atoms on a supporting surface, has been experimentally demonstrated to surpass that of metal particles or clusters in certain scenarios.[26,27] Indeed, several groups have successfully prepared Pt-based SACs to minimize the need for Pt metal while efficiently catalyzing the HER and other reactions.[24,28–31] In general, there are five representative strategies for preparing SACs, namely, the atomic layer deposition,[32] wet-chemistry method,[33] metal–organic framework-derived method,[34] vacancies/defects immobilization,[35,36] and high-temperature atom trapping from bulk particles.[37] However, these methods are associated with significant limitations, including low metal loading, high equipment costs, high pyrolysis temperature, and low yields.[38] Overall, SACs with ultralow loading, high activity, good selectivity, and high atom utilization efficiency (up to 100%) have attracted much attention in various catalytic fields. Developing a simple, facile, and practical approach to synthesizing SAC materials with well-defined sites is particularly promising in the catalysis field. Additionally, catalytic materials are immobilized onto specific substrates to effectively expose their active sites. Conducting polymers such as polyaniline (PANI) are easily prepared in an aqueous medium. Particularly, it is chemically stable and highly conductive in acidic media. More importantly, PANI exhibits efficient protons capture ability from solutions, leading to the formation of protonated amine groups that can be readily electro-reduced for hydrogen generation during the HER process.[39]

In this study, we present a facile and cost-effective in situ electrochemical approach for synthesizing a series of atomically dispersed metal sites on the surface of PANI supported on carbon cloth (PANI-M/CC). The atomically dispersed Pt sites decorated on PANI (PANI-Pt) show superior catalytic performance for the HER, exhibiting an approximately 50-fold increase in mass activity compared to the commercial 20 wt% Pt/C catalyst, along with significantly reduced overpotential. The outstanding performance can be ascribed to the following features: (1) The high electrical conducting properties of PANI provide a low ohmic drop of electron transfer between the catalyst and electrolyte; (2) PANI possesses abundant lone electrons on N atoms, enabling facile capture H^+ ions from solutions and thereby mitigating the influence of coordinating water molecules surrounding H^+, which ultimately benefits the HER, and[40] (3) the atomically dispersed metal sites can maximumly expose their active sites.

2 | RESULTS AND DISCUSSION

As depicted in Scheme 1, the fabrication of PANI-Pt/CC materials includes three steps. A smooth CC was used as a current collector and the substrate for PANI nanofibers growth (Figures S1 and S2). PANI nanofibers were first decorated on the bare CC substrate by electrochemical deposition in an acid aniline solution. As shown in Figure S3, the surface of CC is covered uniformly by PANI nanofibers with diameters of about 200 nm. In addition, the surfaces of the PANI nanofibers are very rough, which is beneficial for the absorption of the metal ions in the subsequent experimental process. After that, the negatively charged $PtCl_6^{2-}$ ions were adsorbed on the positively charged PANI nanofibers via a solution-phase electrostatic assembly and absorption.[40] Finally, the adsorbed $PtCl_6^{2-}$ ions were in situ reduced into atomically dispersed Pt sites under a voltage where hydrogen evolution occurs. The reduction process was conducted with one linear sweep voltammetry (LSV) scan in 0.5 M H_2SO_4 solutions at a scan rate of 2 mV s^{-1}. It is worthwhile to mention that the absence of any other chemical-reducing
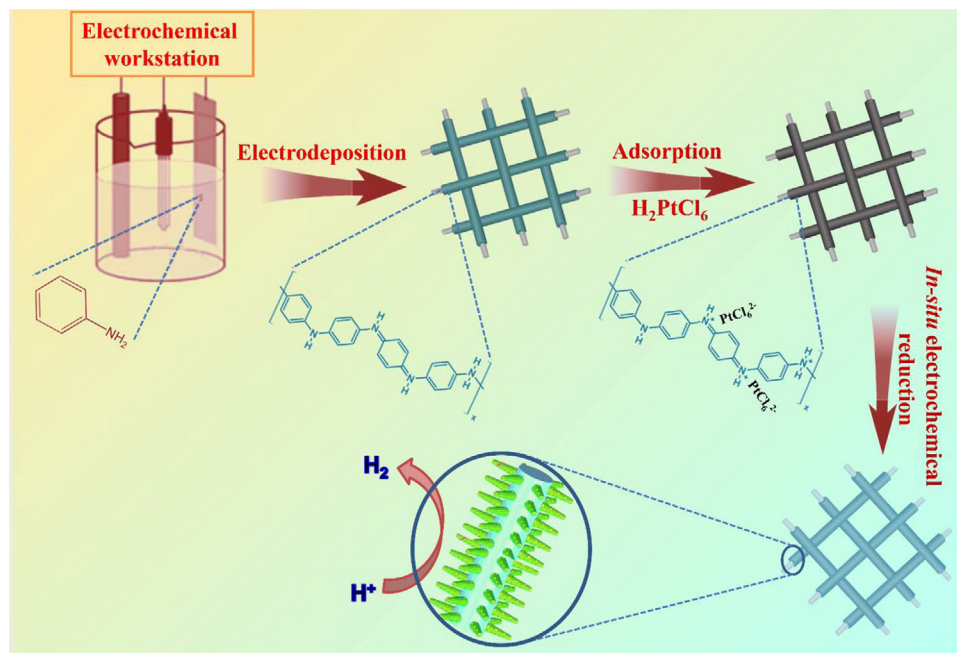
SCHEME 1 Schematic illustration of the synthesis and structure of the PANI-Pt/CC electrocatalyst.

agent would result in a clean surface of the obtained SACs which avoids bringing any side effects and thus offers maximum exposure of active sites.[41]

The structure of the obtained product was initially studied by X-ray powder diffraction (XRD). As shown in Figure S4, no diffraction peaks related to Pt-based clusters or nanoparticles are observed in the XRD patterns of the PANI-Pt-10/CC (10 represents that 10 mg metal salt has been added in the experiment process). The morphology of the prepared sample was characterized using scanning electron microscopy (SEM). As demonstrated in Figure S5, the SEM images at low and high magnifications show that the PANI-Pt-10/CC nanofibers are interconnected to each other, with an average diameter of 200 nm, forming a three-dimensional macroporous structure. The transmission electron microscopy (TEM) and high-resolution TEM images reveal the absence of Pt-based nanoparticles or even clusters in the PANI-Pt-10/CC (Figure S6). The scanning TEM (STEM) images shown in Figure 1A,B indicate that the edge of a PANI-Pt-10 nanofiber is serrated; this phenomenon can enhance the active surface area of the materials, which is further beneficial for improving the catalytic activity.[42] The aberration-corrected high-angle annular dark-field STEM (AC-HAADF-STEM) images of PANI-Pt-10 further confirm the homogeneous distribution of isolated Pt atoms on the PANI nanofiber (Figure S7 and bright dots in Figure 1C,D). The energy-dispersive X-ray (EDX) elemental mapping demonstrates the homogeneous dispersion of N and Pt species on PANI nanofiber (Figure 1E–G). The mass loading of Pt for PANI-Pt-10/CC is measured to be 2.62 μg cm^{-2} through inductively coupled plasma optical emission spectroscopy (ICP-OES) (Table S1).

The chemical state of the Pt in PANI-Pt-10/CC was first investigated using X-ray photoelectron spectroscopy (XPS). The Pt 4f XPS spectrum in Figure 2A presents a single doublet (Pt 4f$_{5/2}$ and Pt 4f$_{7/2}$) at binding energies of 72.9 and 76.1 eV, respectively. The Pt 4f peaks are positioned between those of Pt^{4+} and Pt^0, indicating that the isolated Pt atoms in PANI-Pt-10/CC exhibit a higher positive valence state compared to Pt NPs. The partially charged state observed can be ascribed to the strong interaction between Pt and the PANI molecules, especially through Pt–N ligand bonds.[7,24,43] From the N 1s spectrum (Figure S8A), the trace amounts of N (composed of –NH–, –N =, –N$^+$–) mostly originated from stacked polyaniline. The O 1s peak observed at 532.2 eV can be ascribed to the presence of adsorbed H$_2$O molecules (Figure S8B).[44,45] The electronic and local structure of PANI-Pt-10/CC was further investigated using X-ray absorption fine spectroscopy (XAFS). The Pt L3-edge X-ray absorption near-edge structure (XANES) is presented in Figure 2B, alongside the Pt foil and PtO$_2$ for comparative analysis. The white-line (WL) intensity of PANI-Pt-10/CC is evidently lower than that of PtO$_2$, whereas it significantly surpasses that of Pt foil, further substantiating the oxidation state of Pt$^{\delta+}$ ($4 > \delta^+ > 0$). By fitting the WL intensity, the valence state of the Pt in PANI-Pt-10/CC is calculated to be 2.0 (Figure 2C), thus confirming its oxidation state.[46] Furthermore, the Fourier transform extended X-ray absorption fine structure (FT-EXAFS) spectra of PANI-Pt-10/CC present a prominent peak at approximately 1.8 Å (Figure 2D), which can
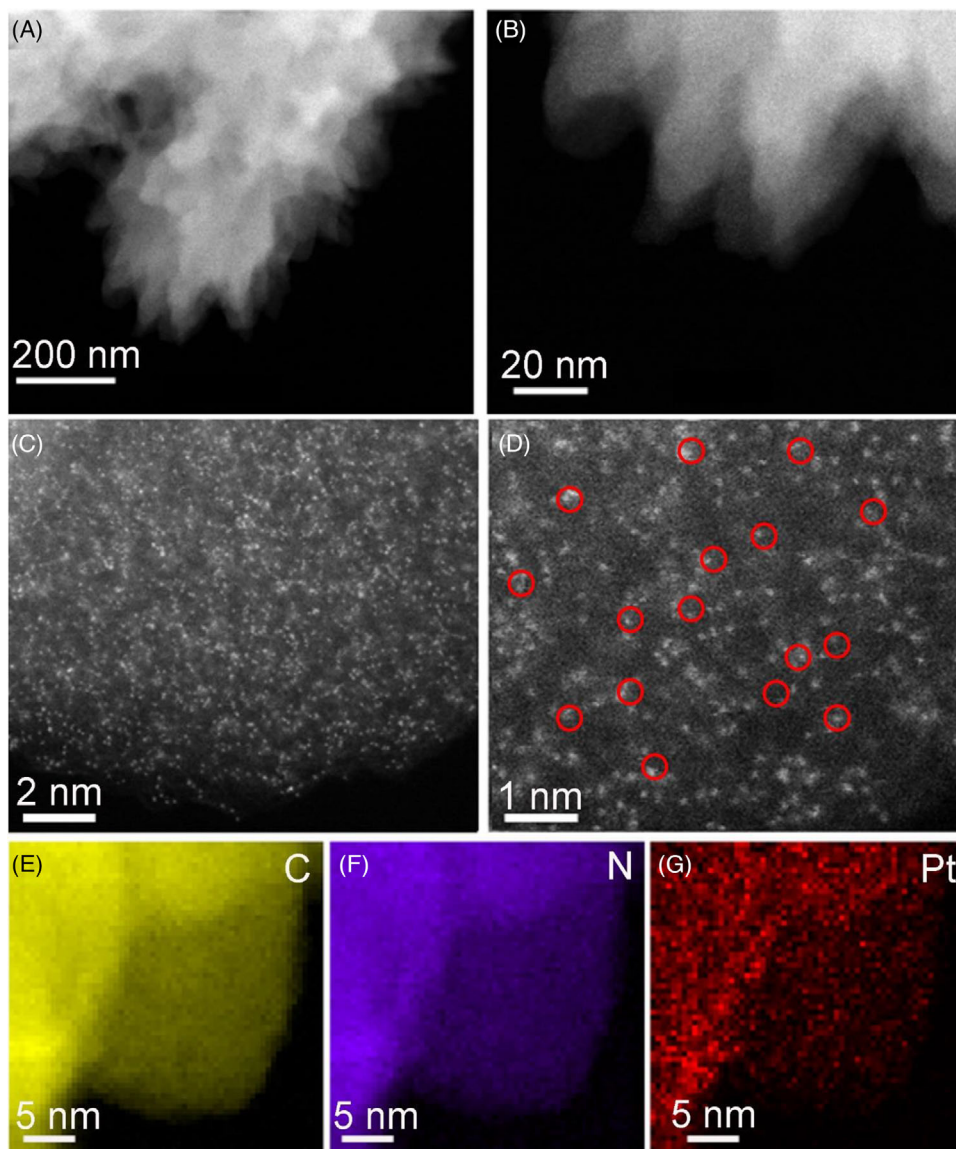
FIGURE 1 (A and B) scanning transmission electron microscopy (STEM) images of PANI-Pt-10 catalyst. (C and D) AC-HAADF-STEM images of PANI-Pt-10 at different magnifications. (E–G) energy-dispersive X-ray (EDX) elemental mapping of C, N, and Pt, respectively, for the PANI-Pt-10 nanofiber.

be ascribed to the Pt–N bond, whereas no obvious Pt–Pt (∼2.7 Å, Figure 2D) or Pt–Cl (∼1.95 Å, Figure S9) peaks are detected in sharp contrast to Pt foil and H_2PtCl_6, respectively. Additionally, the fitting of the main peak and its corresponding parameters can be found in Figure S10 and Table S2. Specifically, the results of the fitting suggest that coordination of single Pt sites by four aniline molecules exhibits the most ideal structures on the carbon cloth surface. These results demonstrate that Pt is atomically dispersed in the PANI nanofiber and anchored by the N atoms with the absence of Pt NPs or clusters.[28] More importantly, the information on Pt–N coordination can be achieved through the analysis of N K-edge XANES results. The pyridinic peak, as shown in Figure S11, exhibits a split into two

distinct peaks (a_1 and a_2), where the presence of a_2 can be ascribed to the bonding of pyridinic N with Pt atoms, consistent with the previous findings.[47,48]

Additionally, a series of PANI-Pt/CC samples with atomically dispersed Pt sites anchored on PANI were obtained with several quantities (5, 20, and 30 mg) of $H_2PtCl_6 \cdot H_2O$. The loadings of Pt in these samples were measured via ICP-OES. As illustrated in Table S1, the Pt content increased in a range between 1.24 and 2.82 µg cm^{-2} and then remained nearly constant even with further addition of $H_2PtCl_6 \cdot H_2O$ by 30 mg. The XRD patterns with SEM and AC-HAADF-STEM images (Figures S12–S15) further indicate that Pt in all obtained samples is atomically dispersed. Furthermore, as shown in Figure S16, the Pt 4f peaks are
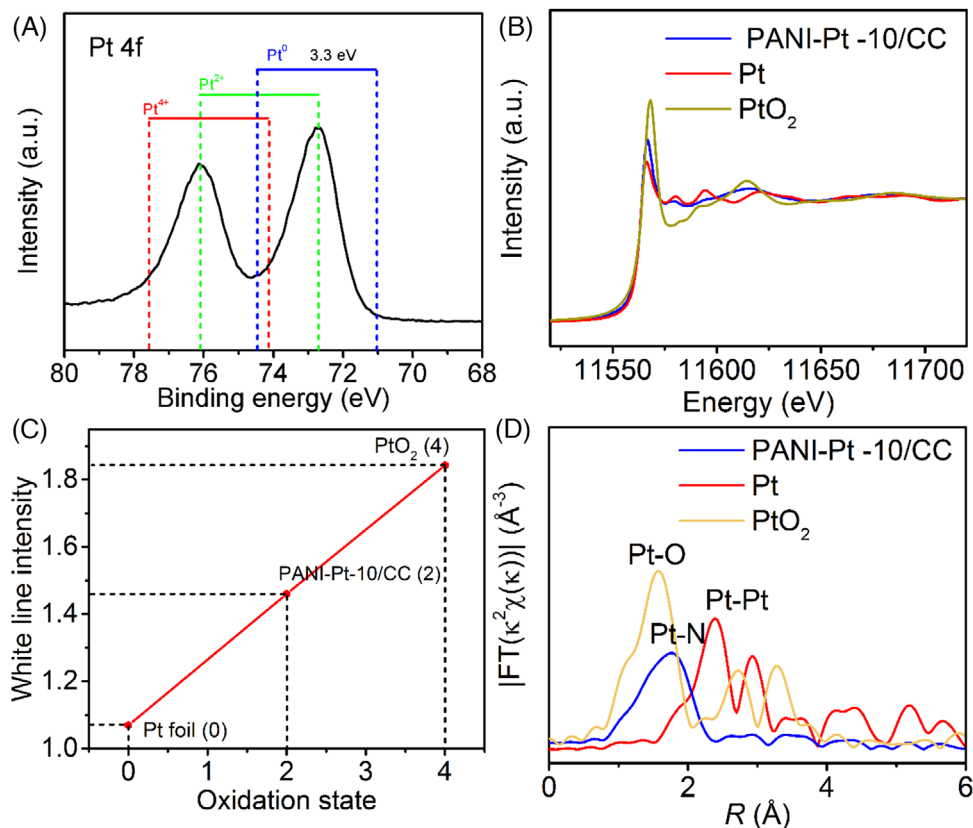
FIGURE 2 (A) High-resolution X-ray photoelectron spectroscopy (XPS) Pt 4f pattern of PANI-Pt-10/CC. (B) The normalized X-ray absorption near-edge structure (XANES) spectra at the Pt L_3-edge for the Pt foil, PtO_2, and PANI-Pt-10/CC. (C) The average oxidation state of Pt in PANI-Pt-10/CC. (D) Corresponding Fourier transform (FT) of EXAFS spectra for Pt foil, PtO_2, and PANI-Pt-10/CC.

located between those of Pt^{4+} and Pt^0, suggesting that the isolated Pt atoms in PANI-Pt-5/CC, PANI-Pt-20/CC, and PANI-Pt-30/CC are an oxidation state. Importantly, this in situ electrochemical strategy can be extended to synthesizing other atomically dispersed metal sites such as Pd and Ru (Figures S17–S20). Therefore, the developed strategy is a universal fabrication approach for atomically dispersing metal sites. This synthetic method has the following unique advantages: (1) The strong protonation of PANI nanofibers results in maximum loading of negatively charged $PtCl_6^{2-}$ ions by adsorption and an electrostatic self-assembly strategy,[43,49] which avoids the anchor of the redundant metal ion, thus no formation of metal clusters and nanoparticles in a subsequent reduction process; (2) the in situ electrochemical reduction is a very simple and fast preparation strategy (as it requires only one LSV scan, Figure S21), without extreme conditions such as high temperature or high pressure, which, in turn, effectively avoids the agglomeration of the atomically dispersed metal atoms.

The electrocatalytic activity of the obtained atomically dispersed Pt samples was evaluated by LSV in H_2-saturated acid media (0.5 M H_2SO_4) at room temperature, employing a scan rate of 2 mV s^{-1}. Before the tests, the saturated

calomel electrode was calibrated in a high-purity H_2-saturated 0.5 M H_2SO_4 solutions electrolyte with a Pt electrode as the working electrode (Figure S22). As depicted in Figure 3A, the LSV curves indicate an increased HER activity when the weight of $H_2PtCl_6 \cdot H_2O$ increased from 5 to 10 mg, whereas the activity tends to be nearly unchanged when further increasing the quantity of $H_2PtCl_6 \cdot H_2O$ to 30 mg. This indicates that the adsorption of negatively charged $PtCl_6^{2-}$ ions on PANI nanofibers has been saturated at 10 mg of $H_2PtCl_6 \cdot H_2O$,[43,45,49] and thus, the excess $PtCl_6^{2-}$ ions cannot be anchored even when further increasing the amount of Pt precursors. To achieve a current density of 10 mA cm^{-2} (j_{10}), the PANI-Pt-5/CC, PANI-Pt-10/CC, PANI-Pt-20/CC, and PANI-Pt-30/CC display overpotentials (η) of 23, 16 (23 mV without iR correction, Figure S23), 16, and 18 mV in 0.5 M H_2SO_4 solutions (Figure 3B), respectively. In addition, the Tafel slope for PANI-Pt-10/CC, PANI-Pt-20/CC, and PANI-Pt-30/CC is nearly 30 ± 2 mV dec^{-1} (Figure 3C), further demonstrating their similar intrinsic catalytic activity. The HER activity of commercial catalyst Pt/C (20 wt%), PANI/CC and blank CC were also investigated for comparative analysis. Similarly, when the catalytic activity is calculated by Pt mass, the PANI-Pt-5/CC, PANI-Pt-10/CC, PANI-Pt-20/CC, and
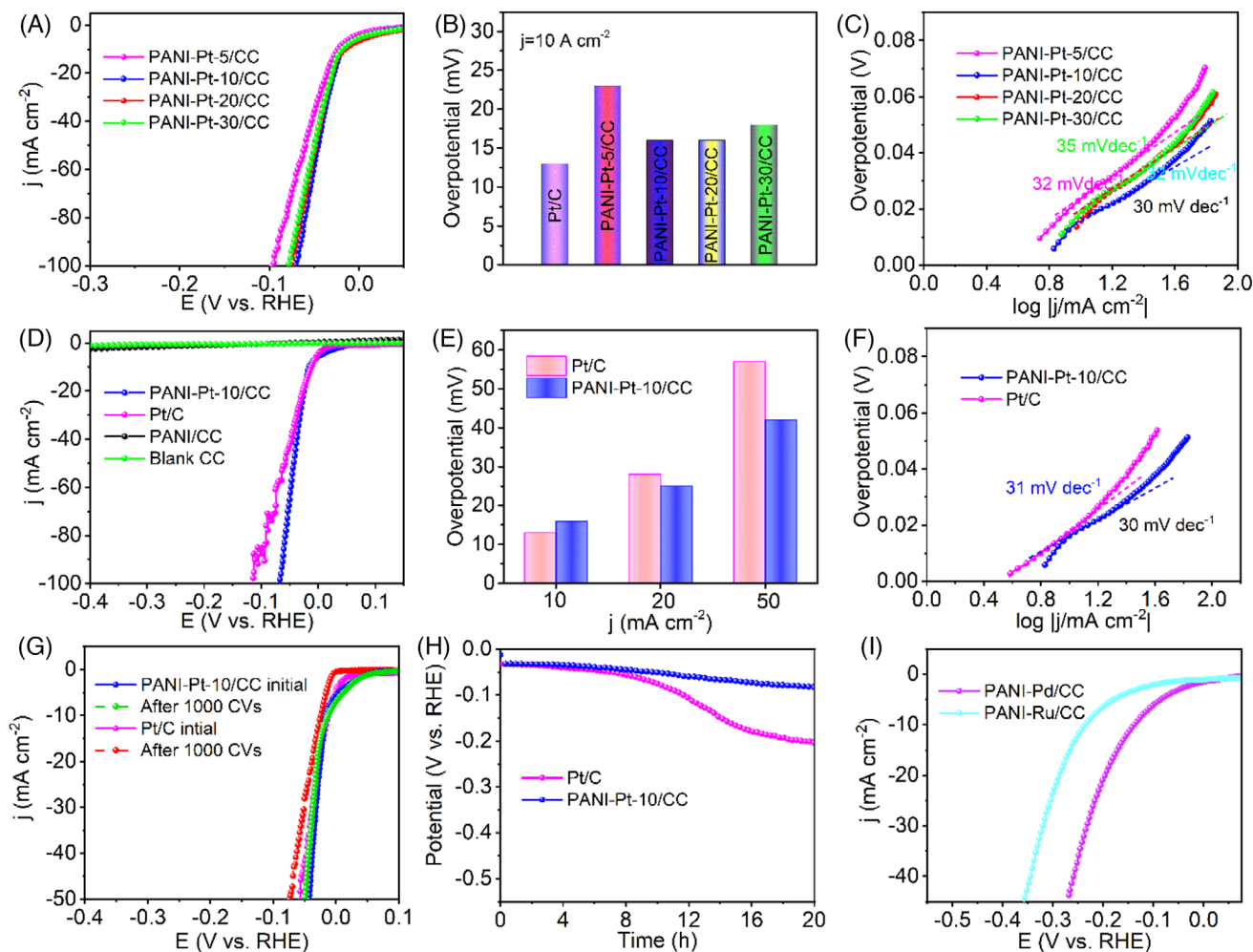
FIGURE 3 (A) Hydrogen evolution reaction (HER) polarization curves of atomically dispersed Pt sites anchored on PANI prepared by different masses of $H_2PtCl_6 \cdot H_2O$. (B) Corresponding overpotentials at $j = 10$ mA cm^{-2}. (C) Corresponding Tafel plots. (D) HER polarization curves of PANI-Pt-10/CC, Pt/C, PANI/CC, and blank CC in 0.5 M H_2SO_4 at a scan rate of 2 mV s^{-1}. (E) Overpotentials at $j = 10$, 20, and 50 mA cm^{-2} of Pt/C and PANI-Pt-10/CC. (F) Tafel plots of PANI-Pt-10/CC and Pt/C. (G) HER polarization curves were recorded before and after 1000 cyclic voltammetry (CV) cycles for PANI-Pt-10/CC and Pt/C in 0.5 M H_2SO_4 solutions. (H) Chronopotentiometric curves of PANI-Pt-10/CC and Pt/C at 10 mA cm^{-2} in 0.5 M H_2SO_4 for 20 h. (I) HER polarization curves of PANI-Pd/CC and PANI-Ru/CC in 0.5 M H_2SO_4 solutions.

PANI-Pt-30/CC show similar mass activities (Figure S24), suggesting that almost all atomic-dispersed Pts were active sites. As illustrated in Figure 3D, blank CC and PANI/CC exhibit poor HER activity, whereas PANI-Pt-10/CC has a better HER activity than commercial Pt/C in the high current density region ($j \geq 20$ mA cm^{-2}) (Figure 3E). Impressively, such impressive HER catalytic activity of PANI-Pt-10/CC is almost among the most active atomically dispersed electrocatalysts in acidic conditions reported so far (Table S3). The Tafel slopes for both PANI-Pt-10/CC and commercial Pt/C are close to 30 mV dec^{-1} (Figure 3F), suggesting the typical Volmer–Tafel mechanism as the HER pathway.[50] The mass activity for PANI-Pt-10/CC is worth mentioning, as it reaches 25 A mg$_{Pt}^{-1}$ at $\eta = 50$ mV, exhibiting a remarkable enhancement 50-fold compared to that

of commercial 20 wt% Pt/C (Figure S25). Additionally, the Nyquist plots in Figure S26 display that the PANI-Pt-10/CC exhibits an exceptionally low solution transfer resistance (R_{ct}) of 2.7 Ω, indicating a rapid electron transfer between the catalyst and electrolyte.[51] In a word, the superior performance of PANI-Pt-10/CC with a much lower Pt loading compared to that of commercial Pt/C electrocatalysts can be explained as follows: (1) The Pt sites are dispersed atomically to maximize the utilization of catalytic sites. (2) The 3D self-supported materials provide a significant specific surface area, thereby optimizing the utilization of catalytic active sites and facilitating efficient mass transport of reactant (H$^+$ ion) and gaseous product (H$_2$). (3) The resistivity of PANI-Pt-10/CC, determined by the four-probe method, is remarkably lower at 3.2×10^{-2} Ω cm compared to that

of 20 wt% Pt/C (1.23 Ω cm), primarily due to the higher conductivity of PANI in comparison to carbon.

It is worth mentioning that the catalyst of Pt NPs on the surface of PANI supported on carbon cloth (PANI-Pt NPs/CC) was prepared through H_2 reduction at 200°C. As illustrated in Figure S27A–C, the SEM and XRD patterns demonstrate that PANI-supported Pt NPs have been successfully obtained. More importantly, the HER mass activity of PANI-Pt NPs/CC exhibits slightly higher performance compared to that of commercial Pt/C catalysts (Figure S27D), which could be attributed to the following reasons: (1) The 3D self-supported materials offer a substantial specific surface area, thereby maximizing the efficiency of catalytic active sites utilization and facilitating efficient mass transport of reactant (H^+ ion) and gaseous product (H_2)[52,53]; (2) benefitting from the lone electron pairs on N atoms, PANI fibers exhibit a remarkable ability to efficiently capture H^+ from solutions, thereby mitigating the influence of coordinating water molecules surrounding H^+ and promoting the HER process. Consequently, PANI-Pt NPs/CC exhibits superior catalytic activity for HER compared to the commercial Pt/C catalyst in acid solutions.[40]

Durability is another pivotal parameter in evaluating HER catalysts. The stability of commercial Pt/C and PANI-Pt-10/CC was evaluated by continuous CV cycles under 0.5 M H_2SO_4 solutions. As shown in Figure 3G, the LSVs for PANI-Pt-10/CC exhibit negligible degradation, whereas commercial 20 wt% Pt/C displays an obvious change. For example, when subjected to 1000 CV cycles at a current density of 10 mA cm^{-2}, the commercial 20 wt% Pt/C exhibits an approximate degradation of ~13 mV in negative potential. Furthermore, the chronopotentiometric curves indicate a slight decline in activity of the PANI-Pt-10/CC catalyst after 20 h in 0.5 M H_2SO_4 solutions (Figure 3H). In other words, both the LSV tests after 1000 cycles and chronopotentiometry experiment demonstrate that the PANI-Pt-10/CC possesses good stability compared to commercial Pt/C. Moreover, the XANES spectra indicate that the WL intensity for fresh and post-HER PANI-Pt-10/CC is almost identical to each other (Figure S28A), further confirming its excellent stability. The FT-EXAFS spectra demonstrate that the bond length and local coordination remain unchanged following the durability test (Figure S28B). Therefore, the origination of excellent HER catalytic stability of PANI-Pt-10/CC can be attributed following reasons: (1) the atomically dispersed Pt sites anchored on aniline effectively prevent detachment, dissolution, redeposition, migration, and agglomeration during catalytic processes, thereby significantly enhancing the stability of PANI-Pt-10/CC.[54–57] (2) The 3D self-supporting porous electrode effectively mitigates the intense H_2 evolution during the HER process, whereas the durability

of powder-like electrocatalysts under HER conditions is compromised as some of the particles may be detached from the electrode.[58] All these results indicate the excellent stability of PANI-Pt-10/CC toward HER in 0.5 M H_2SO_4 solutions. The stability of PANI-Pt/CC, however, exhibited a marginally shorter duration compared to previous reported atomically dispersed Pt anchored on the N-doped carbon materials, such as Pt single-atoms catalysts supported on 3D nitrogen-doped carbon nanotubes, or loaded on N-doped porous carbon nanocages, among others.[59,60] The slightly low stability of PANI-Pt-10/CC compare to other atomically dispersed Pt anchored on the N-doped carbon might be attributed to the variations in the preparation methods. In general, N-doped carbon obtained through high-temperature calcination exhibits higher crystallinity and thus possesses enhanced catalytic stability. Additionally, the Pt–N bond formed during high-temperature calcination might exhibit greater stability and strength than that formed at room temperature.

The PANI-Pt-10/CC material also exhibits good catalytic activity under neutral and basic conditions (Figure S29). It is worth noting that the atomically dispersed metal Ru and Pd on PANI fibers also show a great HER catalytic activity, as illustrated in Figure 3I.

3 | CONCLUSION

In conclusion, a facile and cost-effective in situ electrochemical reduction method was reported for the first time to synthesize a series of atomically dispersed metal (Pt, Ru, Pd, etc.) sites on PANI nanofibers. Taking Pt as an example, the atomically dispersed platinum species anchored on PANI (PANI-Pt/CC) exhibit a higher HER catalytic activity and enhanced durability compared to a commercial Pt/C material in acid solutions. To achieve a current density of 20 mA cm^{-2}, the PANI-Pt-10/CC only requires a minimal overpotential of 25 mV. More importantly, the mass activity for PANI-Pt-10/CC at $\eta = 50$ mV is significantly enhanced, being nearly 50 times higher compared to that of commercial 20 wt% Pt/C. This universal in situ electrochemical reduction strategy opens up a new avenue for the design of atomically dispersed metal sites supported by conducting polymers, carbon materials, and porous materials toward HER and beyond.

4 | EXPERIMENTAL SECTION

4.1 | Materials

All the chemicals were purchased from Sigma-Aldrich (AR grade) and utilized as received without any

additional purification, including aniline, $H_2PtCl_6 \cdot H_2O$, $(NH_4)_2PdCl_4$, $(NH_4)_2RuCl_6$, $HClO_4$, HNO_3, HCl, Nafion (5 wt%), and Pt/C (20 wt%). Ultrapure deionized water (DI Water, 18 MΩ cm^{-1}) was supplied by a Millipore system.

4.2 | Synthesis of catalysts

The electrodeposition method was employed to synthesize PANI using a three-electrode configuration with CC (1×5 cm^2), Ag/AgCl and graphite plate as the working electrode, the reference electrode, and the counter electrode, respectively. The electrolyte was prepared by dissolving 8.0 mL HCl in 88 mL H_2O, followed by the addition of 4.0 mL aniline to achieve a homogeneous solution after stirring for 30 min. Subsequently, a constant potential of 0.8 V versus Ag/AgCl was applied to the CC electrode for a duration of 10 min. Subsequently, the PANI/CC was rinsed with H_2O, followed by drying at 80°C for 1 h and then immersed in different concentrations of $H_2PtCl_6 \cdot H_2O$ solution for 4 h. The $H_2PtCl_6 \cdot H_2O$ solution was prepared with 5, 10, 20, and 30 mg $H_2PtCl_6 \cdot H_2O$ with 20 mL of deionized water. Next, the excess solution is removed and the PANI-H_2PtCl_6/CC hybrid is dried. Finally, the as-prepared PANI-Pt-5/CC, PANI-Pt-10/CC, PANI-Pt-20/CC, and PANI-Pt-30/CC are obtained by in situ electrochemical reduction. The reduction process was conducted with one LSV scan in 0.5 M H_2SO_4 solutions at a scan rate of 2 mV s^{-1}. Note that the PANI-Ru/CC and PANI-Pd/CC were also made under the same condition except for replacing $H_2PtCl_6 \cdot H_2O$.

CONFLICT OF INTEREST STATEMENT

Z.P., G.Z., and S.S. are co-inventors of US patent application no. 63/364,662, "Single-atom catalysts and method of manufacture," related to this work. The remaining authors declare no conflicts of interest. Dr. Shuhui Sun is an Associate Editor of SusMat and a coauthor of this article. To minimize bias, he was excluded from all editorial decision-making related to the acceptance of this article for publication.

ORCID
Gaixia Zhang https://orcid.org/0000-0002-5340-8961
Shuhui Sun https://orcid.org/0000-0002-0508-2944

REFERENCES

1. Coughlin RW, Farooque M. Hydrogen production from coal, water and electrons. *Nature*. 1979;279(5711):301.
2. Lv X, Tian W, Yuan Z. Recent advances in high-efficiency electrocatalytic water splitting systems. *Electrochem Energy Rev*. 2023;6(3):23.
3. Turner JA. Sustainable hydrogen production. *Science*. 2004;305(5686):972-974.
4. Zhao Y, Niu Z, Zhao J, et al. Recent advancements in photoelectrochemical water splitting for hydrogen production. *Electrochem Energy Rev*. 2023;6(2):14.
5. Seh ZW, Kibsgaard J, Dickens CF, et al. Combining theory and experiment in electrocatalysis: insights into materials design. *Science*. 2017;355(6321):4998.
6. Zhang C, Wang F, Batool M, et al. Phase transition of $SrCo_{0.9}Fe_{0.1}O_3$ electrocatalysts and their effects on oxygen evolution reaction. *SusMat*. 2022;2(4):445-455.
7. Bai H, Chen D, Ma Q, et al. Atom doping engineering of transition metal phosphides for hydrogen evolution reactions. *Electrochem Energy Rev*. 2022;5(S2):24.
8. Liu D, Li X, Chen S, et al. Atomically dispersed platinum supported on curved carbon supports for efficient electrocatalytic hydrogen evolution. *Nat Energy*. 2019;4(6):512-518.
9. Chen P, Zhou T, Zhang M, et al. 3D Nitrogen-anion-decorated nickel sulfides for highly efficient overall water splitting. *Adv Mater*. 2017;29(30):1701584.
10. Duan H, Li D, Tang Y, et al. High-performance Rh_2P electrocatalyst for efficient water splitting. *J Am Chem Soc*. 2017;139(15):5494-5502.
11. Zeng L, Zhao Z, Lv F, et al. Anti-dissolution Pt single site with Pt $(OH)(O_3)$/Co (P) coordination for efficient alkaline water splitting electrolyzer. *Nat Commun*. 2022;13(1):3822.
12. Zheng Y, Jiao Y, Jaroniec M, et al. Advancing the electrochemistry of the hydrogen-evolution reaction through combining experiment and theory. *Angew Chem, Int Ed*. 2015;54(1):52-65.
13. Alameda LT, Holder CF, Fenton JL, et al. Partial etching of Al from MoAlB single crystals to expose catalytically active basal planes for the hydrogen evolution reaction. *Chem Mater*. 2017;29(21):8953-8957.
14. Dai Y, Kong F, Tai X, et al. Advances in graphene-supported single-atom catalysts for clean energy conversion. *Electrochem Energy Rev*. 2022;5(S2):22.
15. Tang C, Cheng N, Pu Z, et al. NiSe nanowire film supported on nickel foam: an efficient and stable 3D bifunctional electrode for full water splitting. *Angew Chem, Int Ed*. 2015;54(32):9351-9355.
16. Tian J, Liu Q, Cheng N, et al. Self-supported Cu_3P nanowire arrays as an integrated high-performance three-dimensional cathode for generating hydrogen from water. *Angew Chem, Int Ed*. 2014;53(36):9577-9581.
17. Tang C, Gan L, Zhang R, et al. Ternary $Fe_xCo_{1-x}P$ nanowire array as a robust hydrogen evolution reaction electrocatalyst with Pt-like activity: experimental and theoretical insight. *Nano Lett*. 2016;16(10):6617-6621.

18. Ray C, Dutta S, Negishi Y, et al. A new stable Pd-Mn$_3$O$_4$ nanocomposite as an efficient electrocatalyst for the hydrogen evolution reaction. *Chem Commun*. 2016;52(36):6095-6098.

19. Zhang R, Tang C, Kong R, et al. Al-doped CoP nanoarray: a durable water-splitting electrocatalyst with super high activity. *Nanoscale*. 2017;9(14):4793-4800.

20. Xiao P, Chen W, Wang X. A review of phosphide-based materials for electrocatalytic hydrogen evolution. *Adv Energy Mater*. 2015;4(24):1500985.

21. Li Q, Zou X, Ai X, et al. Revealing activity trends of metal diborides toward pH-universal hydrogen evolution electrocatalysts with Pt-like activity. *Adv Energy Mater*. 2019;9(5):1803369.

22. Liu X, Jiang Y, Huang J, et al. Bifunctional PdPt bimetallenes for formate oxidation-boosted water electrolysis. *Carbon Energy*. 2023;5(12):e367.

23. Ge Z, Ding Y, Wang T. Interfacial engineering of holey platinum nanotubes for formic acid electrooxidation boosted water splitting. *J Energy Chem*. 2023;77(2):209.

24. Li C, Chen Z, Yi H, et al. Polyvinylpyrrolidone-coordinated single-site platinum catalyst exhibits high activity for hydrogen evolution reaction. *Angew Chem Int Ed*. 2020;132(37):16036-16041.

25. Shi W, Liu H, Li Z, et al. High-entropy alloy stabilized and activated Pt clusters for highly efficient electrocatalysis. *SusMat*. 2022;2(2):186-196.

26. Yang XF, Wang A, Qiao B, et al. Single-atom catalysts: a new frontier in heterogeneous catalysis. *Acc Chem Res*. 2013;46(8):1740-1748.

27. Bayatsarmadi B, Zheng Y, Vasileff A, et al. Recent advances in atomic metal doping of carbon-based nanomaterials for energy conversion. *Small*. 2017;13(21):1700191.

28. Yin X, Wang H, Tang S, et al. Engineering the coordination environment of single-atom platinum anchored on graphdiyne for optimizing electrocatalytic hydrogen evolution. *Angew Chem Int Ed*. 2018;57(20):9382-9386.

29. Gong L, Zhu J, Xia F, et al. Marriage of ultralow platinum and single-atom MnN$_4$ moiety for augmented ORR and HER catalysis. *ACS Catal*. 2023;13(6):4012-4020.

30. Zhang J, Zhao Y, Guo X, et al. Single platinum atoms immobilized on an MXene as an efficient catalyst for the hydrogen evolution reaction. *Nat Catal*. 2018;1(12):985-992.

31. Xia C, Qiu Y, Xia Y, et al. General synthesis of single-atom catalysts with high metal loading using graphene quantum dots. *Nat Chem*. 2021;13(9):887-894.

32. Zhang L, Si R, Liu H, et al. Atomic layer deposited Pt-Ru dual-metal dimers and identifying their active sites for hydrogen evolution reaction. *Nat Commun*. 2019;10(1):4936.

33. Wei H, Liu X, Wang A, et al. FeO$_x$-supported platinum single-atom and pseudo-single-atom catalysts for chemoselective hydrogenation of functionalized nitroarenes. *Nat Commun*. 2014;5(1):5634.

34. He T, Chen S, Ni B, et al. Zirconium-porphyrin-based metal-organic framework hollow nanotubes for immobilization of noble-metal single atoms. *Angew Chem Int Ed*. 2018;130(13):3551-3556.

35. Yang Q, Liu H, Yuan P, et al. Single carbon vacancy traps atomic platinum for hydrogen evolution catalysis. *J Am Chem Soc*. 2022;144(5):2171-2178.

36. Wu Z, Zhu P, Cullen DA. A general synthesis of single atom catalysts with controllable atomic and mesoporous structures. *Nat Synthesis*. 2022;1(8):658-667.

37. Jones J, Xiong H, DeLaRiva AT, et al. Thermally stable single-atom platinum-on-ceria catalysts via atom trapping. *Science*. 2016;353(6295):150-154.

38. Qu Y, Chen B, Li Z, et al. Single carbon vacancy traps atomic platinum for hydrogen evolution catalysis. *J Am Chem Soc*. 2019;141(5):4505-4509.

39. Hatchett D, Josowicz M, Janata J. Acid doping of polyaniline: spectroscopic and electrochemical studies. *J Phys Chem B*. 1999;103(50):10992.

40. Feng J, Tong S, Tong Y, et al. Pt-like hydrogen evolution electrocatalysis on PANI/CoP hybrid nanowires by weakening the shackles of hydrogen ions on the surfaces of catalysts. *J Am Chem Soc*. 2018;140(15):5118-5126.

41. Xiong P, Zhang X, Wan H, et al. Interface modulation of two-dimensional superlattices for efficient overall water splitting. *Nano Lett*. 2019;19(7):4518-4526.

42. Wang Z, Hao X, Jiang Z, et al. C and N hybrid coordination derived Co–C–N complex as a highly efficient electrocatalyst for hydrogen evolution reaction. *J Am Chem Soc*. 2015;137(48):15070-15073.

43. Li T, Liu J, Song Y, et al. Photochemical solid-phase synthesis of platinum single atoms on nitrogen-doped carbon with high loading as bifunctional catalysts for hydrogen evolution and oxygen reduction reactions. *ACS Catal*. 2018;8(9):8450-8458.

44. Bao J, Zhang X, Fan B. Ultrathin spinel-structured nanosheets rich in oxygen deficiencies for enhanced electrocatalytic water oxidation. *Angew Chem Int Ed*. 2015;127(25):7507-7512.

45. Ye S, Luo F, Zhang Q, et al. Highly stable single Pt atomic sites anchored on aniline-stacked graphene for hydrogen evolution reaction. *Energy Environ Sci*. 2019;12(3):1000-1007.

46. Jiang K, Liu B, Luo M, et al. Single platinum atoms embedded in nanoporous cobalt selenide as electrocatalyst for accelerating hydrogen evolution reaction. *Nat Commun*. 2019;10(1):1743.

47. Chen P, Zhou T, Xing L, et al. Atomically dispersed iron-nitrogen species as electrocatalysts for bifunctional oxygen evolution and reduction reactions. *Angew Chem Int Ed*. 2017;56(2):610-614.

48. Fang S, Zhu X, Liu X, et al. Uncovering near-free platinum single-atom dynamics during electrochemical hydrogen evolution reaction. *Nat Commun*. 2020;11(1):1029.

49. Sun X, Du Y, Zhang L, et al. Luminescent supramolecular microstructures containing Ru(bpy)$_3$$^{2+}$: Solution-based self-assembly preparation and solid-state electrochemiluminescence detection application. *Anal Chem*. 2007;79(6):2588-2592.

50. Jiao Y, Zheng Y, Davey K, et al. Activity origin and catalyst design principles for electrocatalytic hydrogen evolution on heteroatom-doped graphene. *Nat Energy*. 2016;1(10):16130.

51. Pech D, Brunet M, Durou H, et al. Ultrahigh-power micrometre-sized supercapacitors based on onion-like carbon. *Nat Nanotechnol*. 2010;5(9):651-654.

52. Lu Z, Zhu W, Yu X, et al. Ultrahigh hydrogen evolution performance of under-water "superaerophobic" MoS$_2$ nanostructured electrodes. *Adv Mater*. 2014;26(17):2683.

53. Song Q, Xue Z, Liu C, et al. General strategy to optimize gas evolution reaction via assembled striped-pattern superlattices. *J Am Chem Soc*. 2020;142(4):1857.

54. Zhao L, Zhu J, Zheng Y, et al. Materials engineering toward durable electrocatalysts for proton exchange membrane fuel cells. *Adv Energy Mater*. 2022;12(2):2102665.

55. Pandy A, Yang Z, Gummalla M, et al. A carbon corrosion model to evaluate the effect of steady state and transient operation of a polymer electrolyte membrane fuel cell. *J Electrochem Soc*. 2013;160(9):F972.

56. Zhang C, Wang H, Yu H, et al. Single-atom catalysts for hydrogen generation: rational design, recent advances, and perspectives. *Adv Energy Mater*. 2022;12(27):2200875.

57. Zeng Z, Küspert S, Balaghi S. Ultrahigh mass activity Pt entities consisting of Pt single atoms, clusters, and nanoparticles for improved hydrogen evolution reaction. *Small*. 2023;19(29):2205885.

58. Andronescu C, Barwe S, Ventosa E, et al. Powder catalyst fixation for post-electrolysis structural characterization of NiFe layered double hydroxide based oxygen evolution reaction electrocatalysts. *Angew Chem Int Ed*. 2017;56(37):11258-11262.

59. Wang N, Mei R, Lin X, et al. Cascade anchoring strategy for fabricating high-loading Pt single atoms as bifunctional catalysts for electrocatalytic hydrogen evolution and oxygen reduction reactions. *ACS Appl Mater Interfaces*. 2023;15(24):29195-29203.

60. Pan Q, Wang Y, Chen B, et al. Pt single-atoms on structurally-integrated 3D N-doped carbon tubes grid for ampere-level current density hydrogen evolution. *Small*. 2024;20(25):e2309067. doi:10.1002/smll.202309067

SUPPORTING INFORMATION

Additional supporting information can be found online in the Supporting Information section at the end of this article.